

Analyst

Accepted Manuscript



This is an *Accepted Manuscript*, which has been through the Royal Society of Chemistry peer review process and has been accepted for publication.

Accepted Manuscripts are published online shortly after acceptance, before technical editing, formatting and proof reading. Using this free service, authors can make their results available to the community, in citable form, before we publish the edited article. We will replace this *Accepted Manuscript* with the edited and formatted *Advance Article* as soon as it is available.

You can find more information about *Accepted Manuscripts* in the [Information for Authors](#).

Please note that technical editing may introduce minor changes to the text and/or graphics, which may alter content. The journal's standard [Terms & Conditions](#) and the [Ethical guidelines](#) still apply. In no event shall the Royal Society of Chemistry be held responsible for any errors or omissions in this *Accepted Manuscript* or any consequences arising from the use of any information it contains.



Journal Name

ARTICLE

FTIR imaging of the 3D extracellular matrix used to grow colonies of breast cancer cell lines

Margarita Smolina and Erik Goormaghtigh*

Received 00th January 20xx,
Accepted 00th January 20xx

DOI: 10.1039/x0xx00000x

www.rsc.org/

Infrared imaging was applied to investigate a reconstituted basement membrane, known as Matrigel, in three-dimensional cell cultures. Matrigel, in the vicinity of the colonies, was examined for four breast cancer cell lines presenting different 3D colony morphologies. The MCF-7 and T-47D present mass colonies, SKBR-3 grape-like colonies and MDA-MB-231 stellate colonies associated with more invasive phenotype. The edge of the cell colonies was found to be significantly depleted in Matrigel. Except in a limited number of cases, Matrigel appeared to be thinner at the edges of the colonies but not completely destroyed or torn off as it would be for a purely mechanical effect. When a PCA was run on the spectra of one or several colonies, the score images on PC#3 and PC#4 present structures in the Matrigel areas which appeared as fringes, lines, dots or regular patterns. The effect represents a very small fraction of the total variance but is reproducible for all the 4 cell lines. PC#4 presents systematically a maximum near 1624 cm⁻¹ and a minimum around 1700 cm⁻¹. When spectra are normalized, the effect is less marked but does not disappear. The nature of the variations that exist in the Matrigel layer is therefore not solely related to thickness but also to the chemical composition. At this stage, the weakness of the effect prevents a thorough investigation.

Introduction

Currently, only two-dimensional cultures of cancer cells are widely used. Yet it has been shown that three-dimensional culture matrices are more representative of a tissue environment. More complex culture models have been increasingly developed for studying cancer cell properties.^{1,2} They attempt to mimic “tissue-like” conditions by growing tumor cells in the presence of host stromal cells or extracellular matrix (ECM) proteins, or both.² *In vitro* cancer cells are described to stimulate differentiation of fibroblasts into cancer-associated fibroblasts (CAFs); in turn, CAFs produce growth factors and cytokines that enhance invasiveness.³ This reciprocal feedback also leads to an increase of proteases secretion that promotes ECM degradation and facilitates tumor cell escape. These mechanisms are usually studied by molecular screening of specific markers from *in vitro* cultures or tissue lysate preparations: for example, the expression level of α -smooth muscle actin (α -SMA) for CAFs phenotype,^{4,5,3} the Ki-67 antigen and CD44 adhesion molecules for breast cancer cell proliferative and invasive properties respectively,⁶ and matrix metalloproteinases for ECM degradation.^{1,7} For 3D cultures, a tight correlation has been found between the morphology of

the colonies⁸, gene expression profile⁹ and prognostic indicators.¹⁰ Emerging chemical imaging methodologies based on infrared radiation allow investigating the tumor microenvironment in a rapid, label-free and non-destructive way.

Fourier transform infrared (FTIR) spectroscopy and infrared imaging have already been used to investigate the mutual influence of cancer cells on lymphocytes in tissues,^{3,11} on the extracellular matrix in cancer tissue¹² and on fibroblasts in culture^{3,4,13}. In a previous work, Smolina *et al.* showed that, after Principal Component Analysis (PCA), a score plot indicated that spectra of 2D culture cells formed a distinct cluster, while spectra of 3D culture and clinical carcinoma cells were largely superimposed on PC#1, confirming that the 3D cell culture model is closer to real tissue.¹⁴ The functional and molecular information present in FTIR spectra allowed the characterization of the tumor microenvironment in breast cancer tissues¹¹ and highlighted spectroscopic markers of CAFs in co-culture models.^{15,16} More recently, Holton *et al.* compared the molecular profiling and the infrared spectral features of breast cancer cells as a function of the microenvironment and described the transition of ER+ breast cancer cell lines to a hormone-resistant phenotype under the influence of CAFs.¹³ Many breast cancer cell lines are now thoroughly characterized in 2D and 3D cultures. The availability and relevance of these cell lines (for instance 51 breast cancer cell lines mirroring 145 primary breast tumors¹⁷) have been carefully described for breast cancer.^{18,19} Transcriptomic data are available in both 2D and 3D cultures.

Laboratory for the Structure and Function of Biological Membranes, Center for Structural Biology and Bioinformatics, Université Libre de Bruxelles (ULB), Bld du Triomphe, CP206/02, B-1050 Brussels, Belgium. E-mail: egoor@ulb.ac.be; * corresponding author

Transcription profiling of 25 breast cancer cell lines grown in 2D and 3D tissue culture conditions has been published on the EMBL-EBI website at <http://www.ebi.ac.uk/arrayexpress/browse.html?keywords=E-TABM-244>.

So far, the behavior of the extracellular matrix used for cell culture, in the presence of cancer cell lines, has not been investigated by infrared imaging. In the present work, we use infrared imaging to focus on Matrigel. By Matrigel, we refer to the solubilized tissue basement membrane (BM) extract derived from the Engelbreth-Holm-Swarm mouse sarcoma. It is mainly composed of laminin; other constituents include collagen IV, heparan sulfate proteoglycans and entactin/nidogen.²⁰ It is commonly used as a physiologically relevant model of a laminin-rich BM. Colonies of pure breast cancer cell lines have been grown in a 3D IrECM composed of Matrigel. Matrix in the vicinity of the colonies was examined for four breast cancer cell lines presenting different colony morphologies. The MCF-7 and T-47D present *mass* rounded shaped colonies with a strong intercellular adhesion, SKBR-3 *grape-like* colonies with a poorer cell-cell adhesion and MDA-MB-231 *stellate* colonies distinguished by their invasive phenotype with elongated intercolonial projections.⁹

Materials and Methods

2D cell culture conditions

2D cell cultures were used to maintain and propagate cell lines. Human mammary tumor epithelial cell lines MCF-7, SKBR-3, T-47D and MDA-MB-231 were grown on culture plastic substrate in RPMI 1640 medium (Lonza, Switzerland) supplemented with 10% fetal bovine serum (FBS) (Life Technologies, USA), 2 mM L-glutamine (Lonza, Switzerland), 50 U/mL penicillin and 50 µg/ml streptomycin (Life Technologies, USA) at 37°C in 5% CO₂. Healthy, early-passage (*p* = 3 to 5) and less than 75% confluent cells were used in subsequent 3D culture assays.

3D IrECM culture system

3D cultures were prepared according to the protocol described by Lee *et al.*²¹ Initially, cells were trypsinized from 2D cultures. Single cells were then embedded in Matrigel matrix. 3D embedded culture (*vs* 3D on-top culture) turned out to be more suitable for further handling, providing an increased number of cell colonies in each sample. Briefly, single cells were suspended in 150 µl growth-factor reduced Matrigel basement membrane (BM) matrix (9.6 mg/ml; BD Biosciences, USA) at a density of 0.5-0.7 x 10⁵ cells/ml and plated into eight-well plastic-chambered glass microscope slide (0.7 cm²/well; Corning, USA) precoated beforehand with 50 µl Matrigel. 3D IrECM cell cultures were maintained in H14 medium (see below) with 5% Matrigel, 1% FBS, 50 U/mL penicillin and 50 µg/ml streptomycin at 37°C in 5% CO₂ for 7-13 days with medium change every 2-3 days. H14 medium is prepared on basis of DMEM/F12 (1:1) medium added with 250 ng/ml insulin, 10 µg/ml transferrin, 2.6 ng/ml sodium selenite,

0.1 nM estradiol, 1.4 µg/ml hydrocortisone and 5 µg/ml prolactin.

Formalin Fixation and Paraffin Embedding (FFPE) treatment

After removing plastic dismantled parts, Matrigel matrices with 3D cell cultures on microscope glass slides were fixed in 10% neutral buffered formalin solution for 22 h, followed by dehydration in progressively more concentrated alcohol [50% ethanol – 70% ethanol – 97% ethanol (2x) – absolute isopropanol (3x)], clearing in xylene (3x), infiltration by paraffin (3x) and embedding (200 min protocol in total). Two 4 µm adjacent sections were cut with a rotary microtome: one of them was mounted on a BaF₂ slide (ACM, Villiers Saint Frédéric, France), deparaffinized and intended for IR imaging, the other one was stained with hematoxylin and eosin (H&E) for visual examination. The choice of such a sample treatment has been guided by the purpose of simplifying comparison with tissue samples.

FTIR data acquisition

The FTIR data were collected using a Hyperion 3000 FTIR imaging system (Bruker Optics, Ettlingen, Germany), equipped with a liquid nitrogen cooled 64 x 64 Mercury Cadmium Telluride (MCT) Focal Plane Array (FPA) detector and a 15x objective (NA = 0.4). The data were collected in transmission mode from sample regions of around 170 x 170 µm². Every element of the FPA acts as an independent and discrete detector from which a full spectrum is obtained. The corresponding pixel covers an area of 2.7 x 2.7 µm². One FTIR image (unit image) results in 4096 spectra, each one being the average of 256 scans recorded in a spectral range from 3800 to 900 cm⁻¹ (ca. 5 minutes). To cover larger sample areas, several FTIR images were tiled in order to obtain one FTIR map. The background spectrum, acquired as the average of 512 scans in the absence of sample or BaF₂ slide. The spectral resolution was set to 8 cm⁻¹.

Experiments were performed in triplicate, independently for all cell lines from cell thawing to FTIR data acquisition.

Data analyses

Pre-processing of IR spectra

When indicated, spectra were preprocessed as follows. The spectra were baseline-corrected. Straight lines were interpolated between the spectra points at 3736 3648 3006 2812 2404 2164 1870 1770 1734 1480 1274 1140 984 and 912 cm⁻¹ and subtracted from each spectrum. Spectra were normalized for equal area between 1734 and 1480 cm⁻¹ (Amide I and II peaks). Visual inspection of spectra as well as systematic screening for negative lobes on the left-hand side of the Amide I band did not reveal significant dispersive artifacts.²²⁻²⁶ As Mie scattering corrections rely on simplified models and as dispersive artifacts were minor in the present work, we preferred not applying such a correction. Derivation calculation did not provide more efficiency as also reported elsewhere²⁷ and was not applied to preprocessed IR spectra.

Statistical analyses of IR spectra

Unsupervised PCA analyses were performed. These multivariate methods enable variable reduction by building linear combinations of wavenumbers varying together, called Principal Components (PC). Usually 2 to 6 PCs are sufficient to explain the major proportion of the original variance of the dataset, reducing the description of every spectrum to 2 to 6 numbers representing its scores on the PCs.

Correction of the IR spectra for water vapor and atmospheric CO₂ contribution, baseline subtraction, normalization, application of quality filters and PCA analyses were carried out

by Kinetics, a custom-made program running under Matlab (Mathworks, Inc.).

Results

In the present work, Matrigel containing the colonies was processed according to the usual FFPE protocol (see *Materials and Methods*). 4- μm thick deparaffinized sections are examined here.

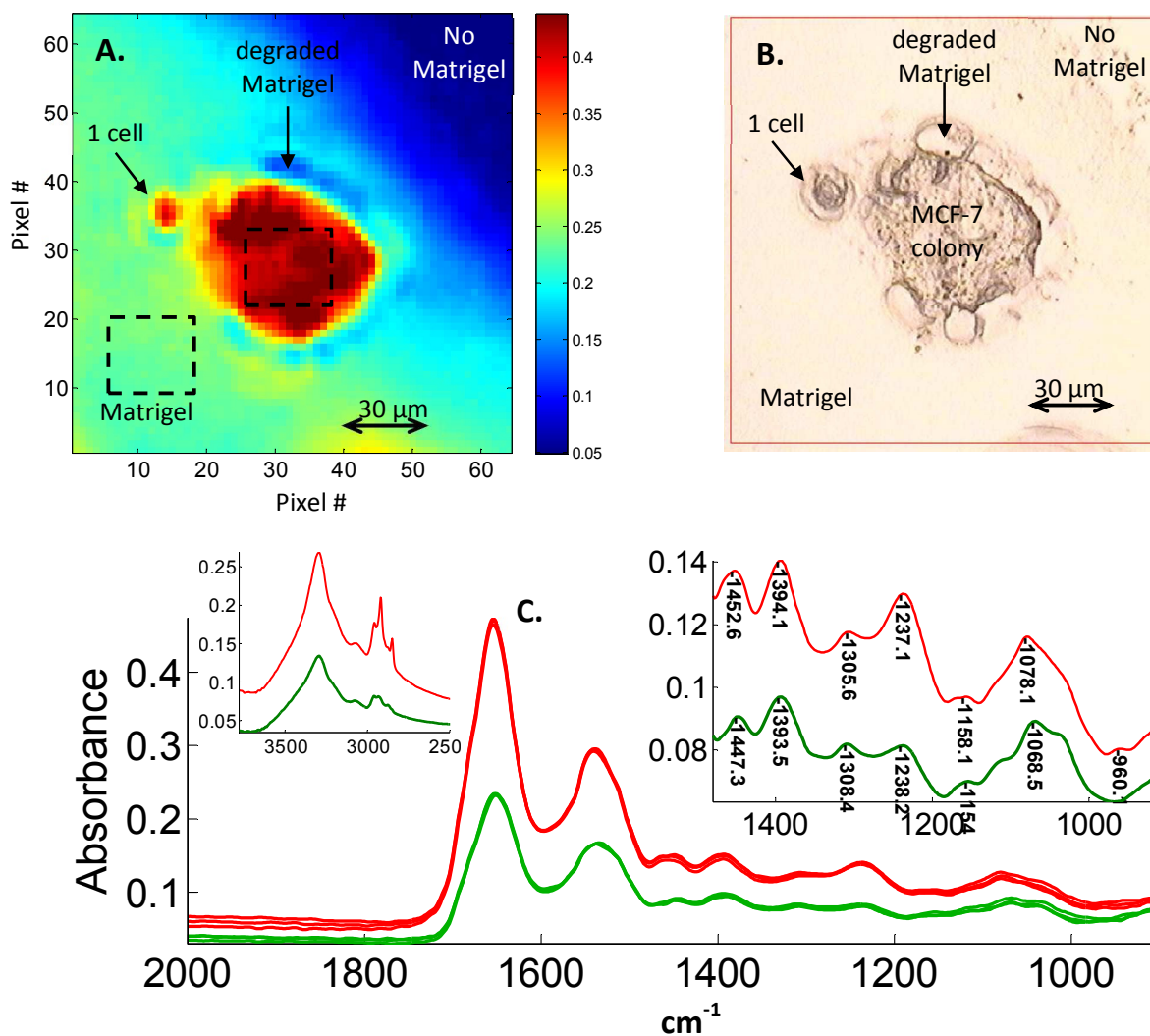


Figure 1: Illustration of the quality check. **A.** FTIR image obtained by plotting the absorbance at 1654 cm^{-1} (64×64 pixels, $2.7 \times 2.7\ \mu\text{m}^2$ each), prior to any processing, of a section of a 10 day-old colony of MCF-7 cell line grown in a 3D Matrigel matrix. **B.** Bright field view of the same image. **C.** Three spectra collected from the cell colony (red) and three spectra from Matrigel (green). The left inset reports an enlargement between 3780 and 2500 cm^{-1} and the right inset between 1480 and 900 cm^{-1} for the mean of the spectra present in the two squares (dashed lines in A.) for the colony (red) or Matrigel (green).

Figure 1 illustrates the infrared imaging of a 10 day-old MCF-7 colony and its microenvironment. The colony, embedded and grown in 3D Matrigel matrix, was fixed in 10% neutral buffered formalin solution, dehydrated in progressively more

concentrated alcohol solutions, embedded in paraffin, cut in $4\text{-}\mu\text{m}$ sections and deparaffinized. The dewaxed section was deposited on a BaF₂ slide. A picture of the sample was obtained under bright light (Figure 1B) and acquired by

infrared imaging between 3900 and 900 cm^{-1} (Figure 1A) on the same section. The infrared data set contains 64 x 64 spectra. The absorbance at 1654 cm^{-1} is reported in Figure 1A. It can be observed on both Figures 1A and 1B that the Matrigel layer is thinner near the contact with the colony. This is also true for the single cell observed on the left side of the figure.

In the core of the colony, the absorbance of Amide I at 1654 cm^{-1} reaches about 0.4, while it is only ca. 0.25 for Matrigel. Three spectra randomly selected from the cell colony and three spectra collected from Matrigel area are reported in

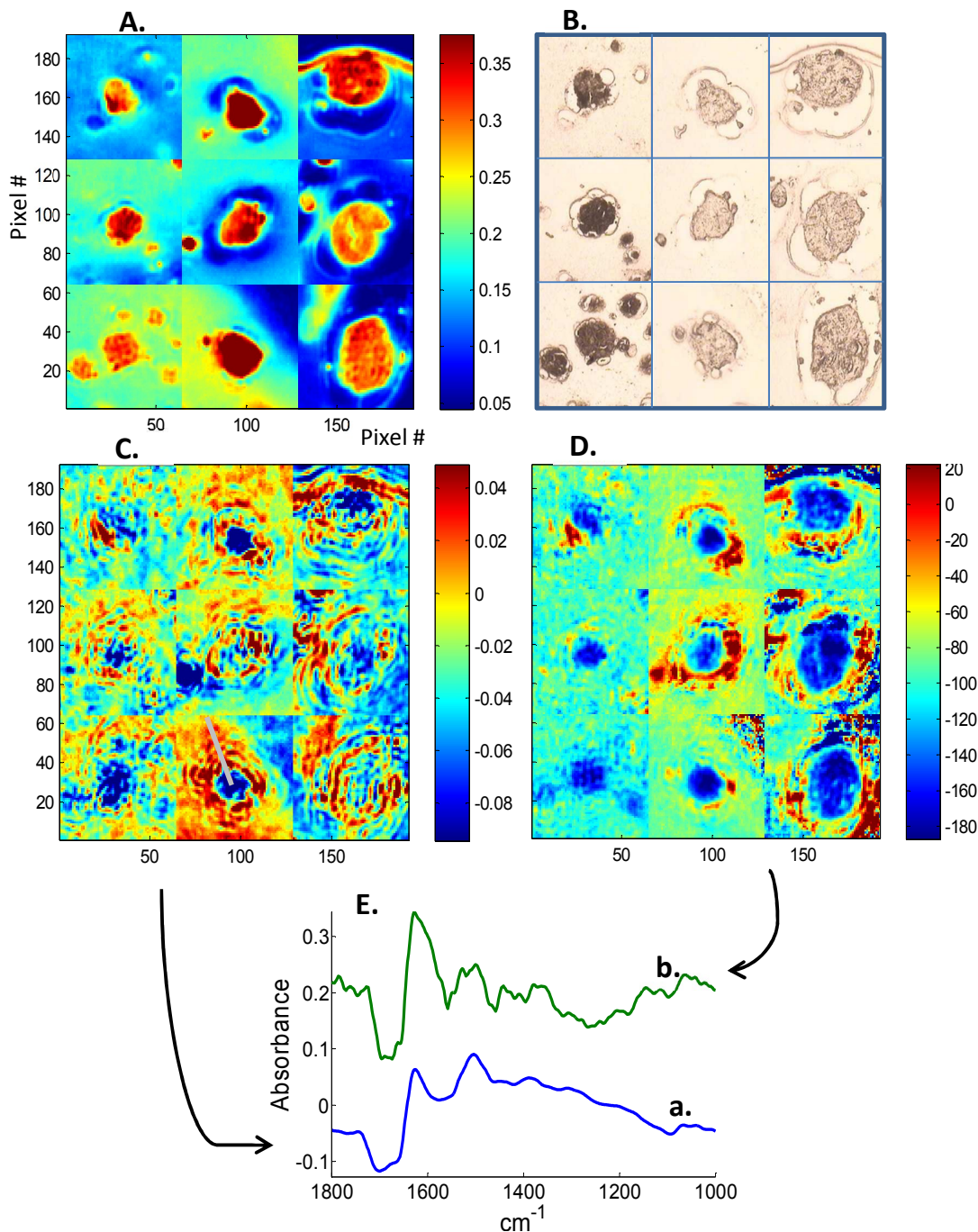


Figure 2: Analysis of nine images of MCF-7 colonies grown embedded in Matrigel for 7 days (first column) and 10 days (second and third columns of each image, two independent cultures). Each column corresponds to an independent culture. Each image within one column represents colonies belonging to the same culture. The nine images have been merged in a single dataset and analyzed together. Except for panel D., no processing was applied. A. Absorbance at 1654 cm^{-1} . B. Bright field images. C. Score of the spectra on the 4th principal component. D. Score of the spectra on the 4th principal component after baseline subtraction and normalization of the spectra as explained in *Materials and Methods*. E. 4th principal component obtained from panel C. (trace a) and from panel D. (trace b, offset for better readability) as indicated by the arrows. The grey line in panel C. indicates here spectra that have been collected for construction of the Figure 3.

Figure 1C. They illustrate the intensity difference and the level of variability found among individual spectra. Amazingly, the left inset in Figure 1C (mean of ca. 200 spectra collected from the colony or from Matrigel) reports that the methylene group content identified by the stretching vibrations $\nu_{as}(\text{CH}_2)$ at 2918 cm^{-1} and $\nu_s(\text{CH}_2)$ at 2950 cm^{-1} is very significantly more intense in the colony than in Matrigel. The right inset in Figure 1C shows an enlargement of the $1480\text{--}900\text{ cm}^{-1}$. Beside the intensity difference already mentioned, it can be observed that some peaks are different, in particular the bands at 1078 cm^{-1} and 1237 cm^{-1} are more intense in the colony than in Matrigel. These two bands are usually associated with asymmetric and symmetric phosphate (PO_2) stretching respectively.

Figure 2 reports the analysis of nine colonies of MCF-7 cells grown in Matrigel. The images presented in Figure 2 have been obtained by tiling 64×64 pixels unit images, where each column corresponds to an independent culture. Figure 2A reports the absorbance at 1654 cm^{-1} , i.e. a marker of the protein content. No processing was applied to the spectra. The corresponding image obtained in bright light is presented in Figure 2B. When a PCA is run on these unprocessed data (all together), PC#1 (93% of the total variance) and PC#2 (5% of the total variance) account for scaling and baseline shifts. The score plot image on these PCs (not shown) is very similar to the absorbance image shown in Figure 2A. Scores PC#3 (1.0% of the total variance) and PC#4 (0.35% of the total variance)

produces images with irregular fringes in Matrigel. This is illustrated for PC#4 in Figure 2C and the corresponding PC is plotted in Figure 2E, trace a. In order to check whether this could be due only to baseline shifts or thickness changes, the same data set was pre-processed with baseline subtraction and scaling as described in *Materials and Methods*. Figure 2D reports the score image obtained for PC#4. PC#4 has been plotted in Figure 2E, trace b. It presents some similarities with the PC#4 obtained previously on unprocessed spectra, particularly in the $1800\text{--}1400\text{ cm}^{-1}$ interval. The image obtained with pre-processed spectra show less marked fringes but some structure remains visible in Matrigel. When spectra (Figure 3A) are collected along a line crossing the colony and different fringes (drawn in Figure 2C), the profile of absorbance at 1622 cm^{-1} drops sharply over ca. 5 spectra ($13\text{ }\mu\text{m}$) when following the line from inside the colony to the outside (Figure 3B). Enlarging the Matrigel contribution profile (Figure 3C), it shows a minimum close to the colony; then, when moving away from it, this contribution increases but with some fluctuations. These fluctuations are responsible for the fringe-like structures observed in Figure 2. The drop at the edge of the colony and the fluctuations in the bulk of Matrigel are almost systematically observed when this analysis is repeated around the different colonies (not shown). Relative disappearance of Matrigel at the edge of the colony can even be observed on the absorbance images such as in Figure 1A or Figure 2A.

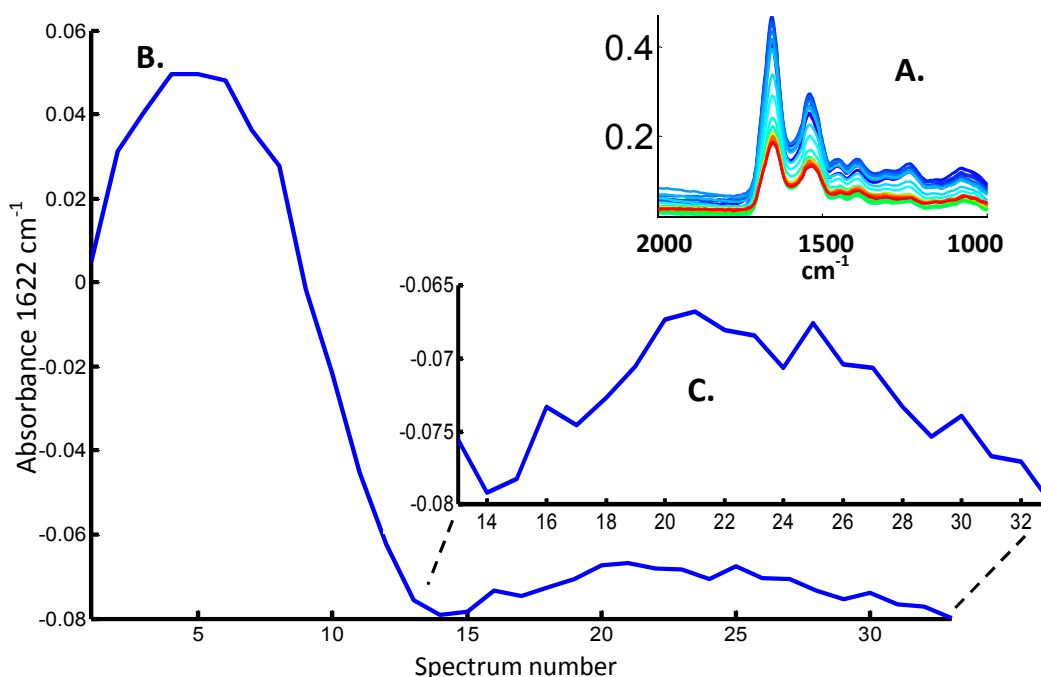


Figure 3: Absorbance (centered at 0) profile at 1622 cm^{-1} describing the movement from the center of a colony into the ECM. Spectra have been collected along the grey line drawn in Figure 2C (bottom). A. A set of 35 spectra selected along the line passing from the center of the colony (blue) to the outside (red). B. Absorbance (centered at 0) at 1622 cm^{-1} as a function of the spectrum number. C. Enlargement of a portion of B (region outside the colony).

At this point, it was of interest to investigate whether the patterns observed in Matrigel were related to a particular behaviour of MCF-7 cell line or whether they would also be observed for other breast cancer cell lines. Figure 4 demonstrates the PCA analysis for three other cell lines: MDA-MB-231, T-47D and SK-BR-3. Nine colonies from three

independent cultures are represented for each cell line. While the images reporting the absorbance at 1654 cm^{-1} give a clear view of the morphology of the colonies, imaging the scores on PC#4 shows in each case a patterned image similar to the ones observed for MCF-7 colonies. A bright field image of the colonies is presented in Figure S3

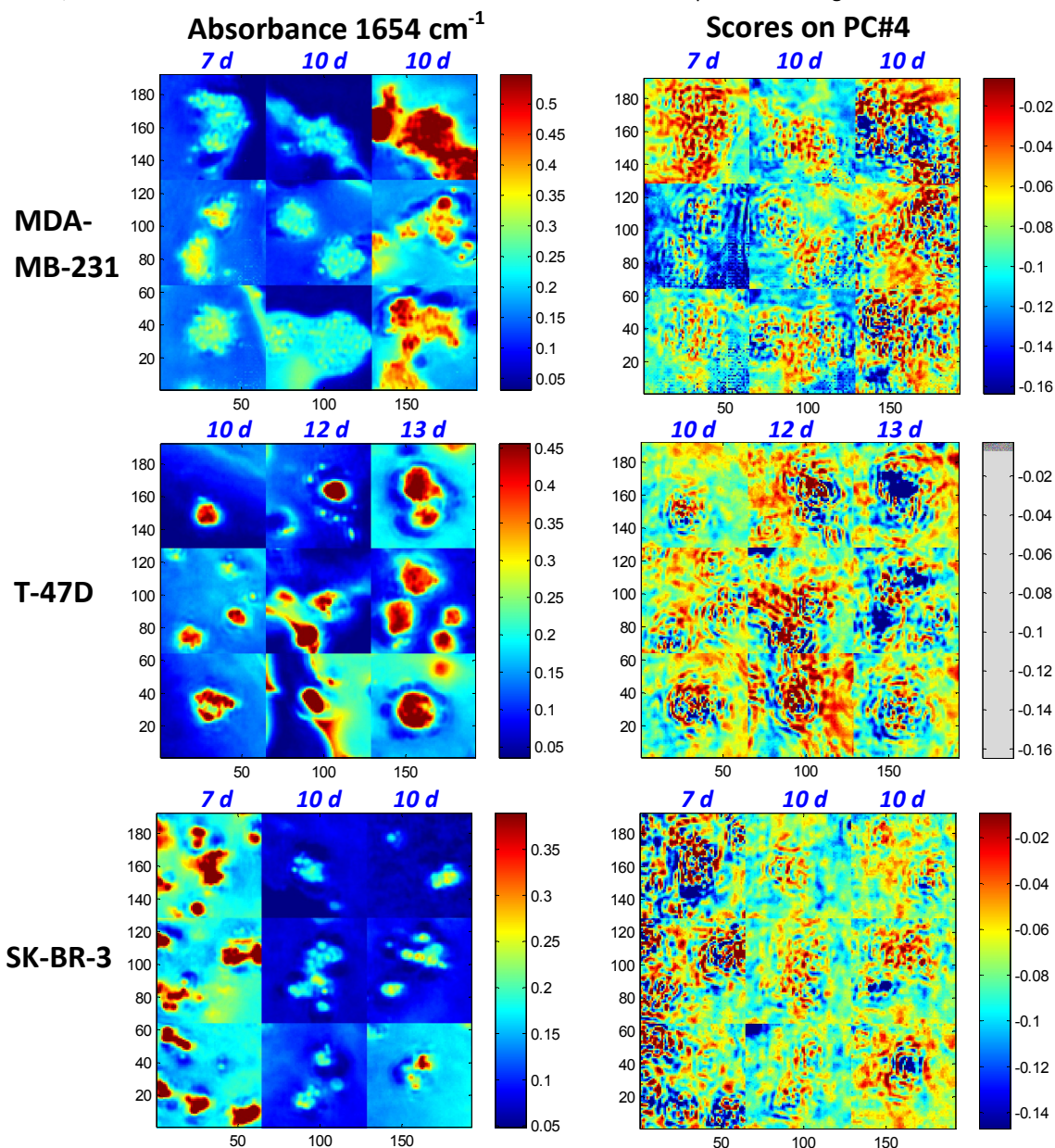


Figure 4: Absorbance (at 1654 cm^{-1}) and PCA (scores on the 4th PC) for three cell lines: MDA-MB-231, T-47D and SK-BR-3. Each column corresponds to an independent culture, each image within one column represents colonies belonging to the same culture. For each cell line, nine images have been merged into a single dataset and analyzed together by PCA. No processing was applied to the spectra. The age of the colonies in days is indicated in blue on top of each column. Corresponding bright field images of the colonies are reported in Figure S3.

As a control Matrigel sections from gels obtained in the absence of cell colony were analyzed. Results are reported in Figure S1 (Supplementary Materials) Figure S1 reports for 3 samples of Matrigel A. the absorbance image, B. the score

image on PC#4 obtained after PCA on the $1800\text{-}1000\text{ cm}^{-1}$ spectral region and C. the score image on the PC#4 obtained in Figure 2A, trace a., forcing the recognition of the features responsible for the patterns shown in this paper. Figure S1

convincingly demonstrates that the patterns observed are not present when pure Matrigel is processed in the same way.

When all data are gathered into a single analysis, the patterns observed previously remain present and PC#4 shows strong similarities with the ones obtained for single cell lines. Such an analysis is presented in Figure 5 (top) for 12 independent

cultures which included the four cell lines: MCF-7, MDA-MB-231, T-47D and SK-BR-3. The shape of PC#4 (Figure 5, bottom) is rather similar to the one presented in Figure 2E (trace a) for MCF-7 alone.

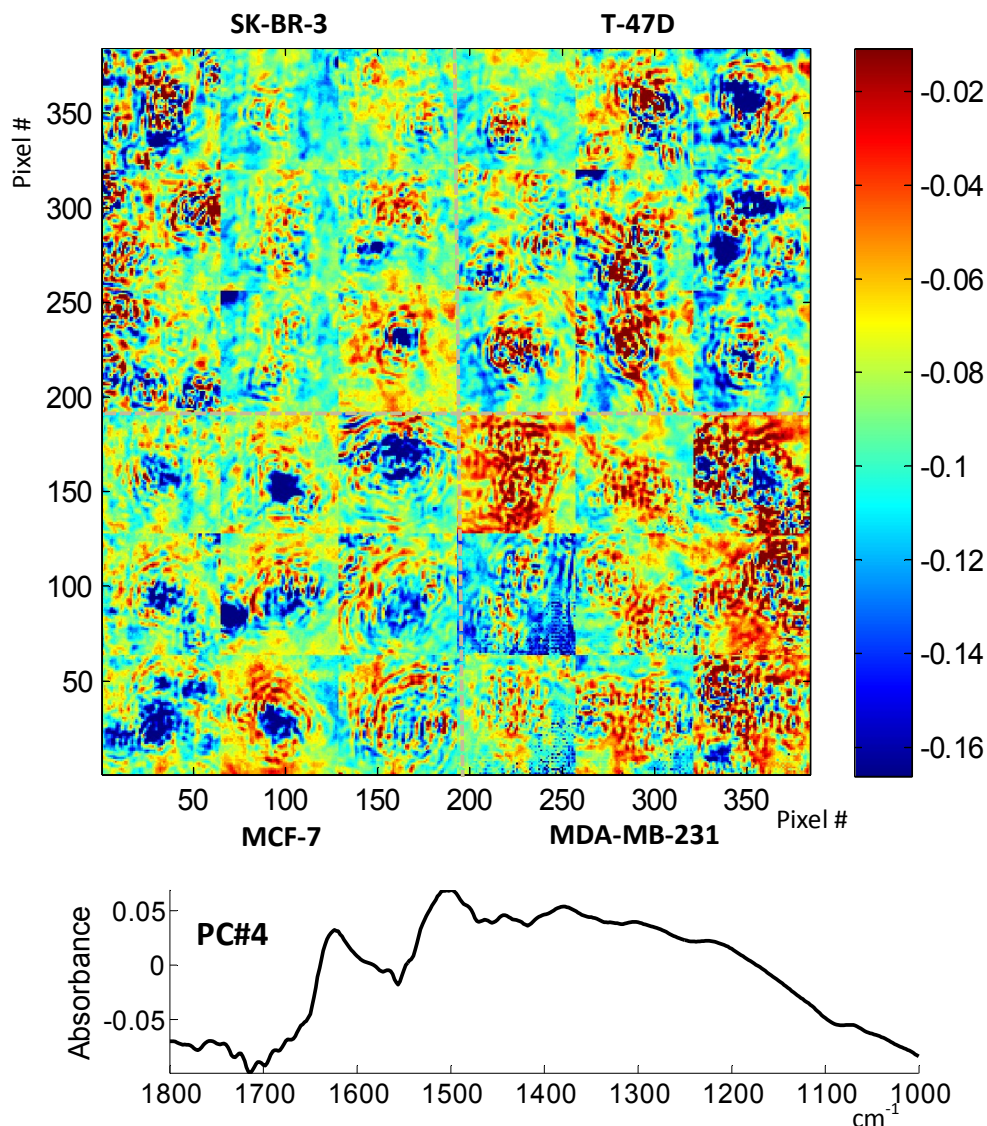


Figure 5: Simultaneous PCA analyses ($1800\text{-}1000\text{ cm}^{-1}$) of 36 infrared images (147,456 spectra) corresponding to 12 independent cultures of 4 cell lines (3 cultures/cell line; 3 IR images/culture): MCF-7, MDA-MB-231, T-47D and SK-BR-3. Top: scores of each spectrum on PC#4; bottom: shape of PC#4. No processing was applied to the spectra.

Discussion

The rationale for growing cells in 3D culture is to provide them with a possibility to interact among them as well as with the extracellular matrix components through dedicated proteins, as it is the case in tissues.²⁸ If necessary, co-cultures of breast cancer cells can be considered with fibroblasts^{4,13,29-31} and lymphocytes^{29,32,33} and, in that way, they regulate cell proliferation, migration and apoptosis. In 3D cultures, cells interact with extracellular matrix and are more similar to cells

found in tissues.²¹ Growing cells in 3D *in vitro* cultures also offers the opportunity to study the impact of well-characterized cell lines on the Matrigel matrix, composed essentially of laminin, collagen IV and other components of the basal membrane.

In the present work, 4- μm thick deparaffinized sections of Matrigel containing the cell colonies were studied. This choice could be discussed as chemical modifications of the sample are introduced by the FFPE processing³⁴ in all the major cell

constituents.^{35–38} The influence of formalin-based fixation and paraffin preservation on spectral features of tissues and cells has been investigated, in particular by infrared and Raman spectroscopies.^{34,39–43} While some studies report only a slight impact of formalin fixation on the spectra,^{42–45} other studies observed important modifications concerning the cellular lipid and protein content.^{34,46,47,41} Despite these chemical modifications, this technique allows the precise identification of the different cell types present in biopsied tissues^{48,49,11} indicating that the FFPE process preserves spectral differences between distinct cell types, in agreement with studies carried out on pure cell lines.⁵⁰ In turn, the full potential of infrared spectroscopy can be used to identify whether changes occur in the sample, where they occur and when they occur. This is a first exploratory step. Identifying precisely the molecules responsible for the changes is another step for which FFPE could be a problem. It must be added that FFPE procedure is routinely used in the clinic and most tissue banks are still presently FFPE processed. Comparison of 3D-grown cultures and clinical samples therefore rely on FFPE-processed samples. Alternatives to FFPE processing such as cryosectioning are available but such procedures also alter the sample as already demonstrated by Shim and Wilson in 1996.⁵¹

Four breast cancer cell lines have been grown in a laminin-rich extracellular matrix or Matrigel. Matrigel is essentially composed of basal membrane proteins and proteoglycans. Comparison of the spectra of cell colonies and Matrigel indicates that the bands at 1076 cm^{-1} and 1238 cm^{-1} , usually assigned to PO_2 stretching vibrations $\nu_s(\text{PO}_2)$ and $\nu_{as}(\text{PO}_2)$, are more intense inside the colony but are still present in Matrigel. To address the question of the origin of these two bands in bulk Matrigel, Matrigel films were obtained prior to any step involved in FFPE processing. When fresh Matrigel was dried and IR images recorded, these two bands were already present. Figure S4A and B present the mean spectrum of untreated, just dried, pure Matrigel (trace in green). It clearly demonstrates that the absorptions around 1078 cm^{-1} and 1237 cm^{-1} are already present before any processing. The contribution of fixation by neutral buffered formalin solution can therefore not be associated here with these bands. Quite surprisingly, there is also a huge difference in the methylene group vibrations $\nu_{as}(\text{CH}_2)$ at 2918 cm^{-1} and $\nu_s(\text{CH}_2)$ at 2950 cm^{-1} . Figure 1C reveals that a very large contribution from the CH_2 groups is present in the spectra of the colonies while the spectra of Matrigel contain only a small contribution similar to what can be observed in the spectra of pure proteins.^{51–53} The origin of long hydrocarbon chains in the colonies could be due either to the presence of cell lipids which were not removed upon dewaxing or to some paraffin left in the sample. It is difficult to believe that for a $4\text{-}\mu\text{m}$ thick section, paraffin would be significantly retained in the cells but not in the Matrigel. Yet, at this stage we cannot completely rule out the presence of paraffin. Using deuterated paraffin could help resolve this issue.

The difference between the features observed in the presence and absence of colonies needs to be briefly discussed. There

are always “patterns” in the images. In the absence of colonies, the features that are observed are disorganized. What is specific to the presence of colonies is that PC4 images show lines, usually concentric around the colonies. For some images, it is perfectly clear, for others, it is less obvious but a close examination of the images reveals some concentric features. By showing results on 4 cell lines and 9 images per cell line, we show this variability. For instance, concentric lines are quite clear for the rather large MCF-7 colonies as shown in Figure 2C. Such patterns are never observed in the absence of colonies as illustrated in Figure S1. Figure S1 displays cloudy, irregular, random shapes but nothing similar to the series of lines observed in Figure 2C. Figure S2 compares Matrigel in the presence of a large colony, a small colony and no colony. There is no regular line in the absence of colony, almost none for the small colony and significant ones for the large colony. It is important to underline that, even though the origin of the regular patterns observed remains unknown, infrared imaging was shown here to be very efficient in exploring minute variations in tissue-like samples. Discovering unexpected features such as the ones presented here would be very unlikely with any other methods.

Cell matrix remodeling is part of the living process. It plays a major role in wound healing and cancer metastasis. In tissues, it has been shown using infrared imaging that the extracellular matrix is different in wound and in the ECM in intimate contact with carcinoma.¹¹ Furthermore, an effect of the tumor on the ECM was shown to decay with the distance from the tumor.¹² Only a few studies have been carried out on a simplified *in vitro* model. Chiu *et al.*⁵³ applied image spatial correlation to collagen second harmonic generation images and demonstrated that collagen density around MDA-MB-231 and MCF-7 was modulated by the cells. The present work reveals that an originally homogenous cell matrix such as Matrigel does not remain a layer of uniform thickness and uniform chemical composition after breast cancer cell lines have grown in it for 7–12 days. First, the edges of the cell colonies are significantly depleted in Matrigel in agreement with data reported in Figure 3. This phenomenon needs to be further investigated. It can be either due to an enzymatic digestion by enzymes secreted by the colonies or to a mechanical stress. Except in a limited number of cases, Matrigel appears to be thinner at the edges of the colonies but not completely destroyed or torn off as it would be for a purely mechanical effect. When a PCA was run on the spectra of one or several colonies, the score images on PC#3 and PC#4 present structures in Matrigel areas such as fringes, lines, dots or regular patterns. It must be stressed that such patterns are only apparent for score images representing the score plots on the 3rd or 4th PC. In the case of Figure 5, PC#4 describes only 0.19% of the total variance. We are therefore observing a very minor effect. Yet, it is reproducible for four cell lines and PC#4 demonstrates systematically a maximum near 1624 cm^{-1} and a minimum around 1700 cm^{-1} . In order to evaluate to which extent ripple in the Matrigel layer could be responsible for this effect, spectra have been corrected for baseline and scaled to

a same area under the Amide I and Amide II. This processing does remove part of the patterning but some of it remains. Furthermore, PC#4 shape in the 1800-1400 cm⁻¹ spectral range has strong similarities with the one obtained before any processing (Figure 2). The nature of the variations that exist in the Matrigel layer is therefore not solely related to thickness but also to chemistry. At this stage, the weakness of the effect prevents a thorough investigation.

Acknowledgements

This research has been supported by grants from the National Fund for Scientific Research (FRFC 2.4527.10, 2.4526.12 and T.0155.13). E.G. is Research Director with the National Fund for Scientific Research (FNRS) (Belgium), M.S. is Research Fellow supported by grant T.0155.13 from the FNRS (Belgium).

Abbreviations

2D/3D: two-/three-dimensional, α -SMA: α -smooth muscle actin, BaF₂: Barium Fluoride, BM: basement membrane, CAFs: cancer-associated fibroblasts, Extracellular Matrix, FFPE: formalin-fixed, paraffin-embedded, FPA: Focal Plane Array, FTIR: Fourier Transform Infrared Spectroscopy, H&E: hematoxylin-eosin, IrECM: laminin-rich extracellular matrix, MCT: Mercury Cadmium Telluride, PC: Principal Component, PCA: Principal Component Analysis, S/N: signal-to-noise ratio

References

- Z. M. Che, T. H. Jung, J. H. Choi, D. J. Yoon, H. J. Jeong, E. J. Lee, and J. Kim, *Biochem. Biophys. Res. Commun.*, 2006, **346**, 268–75.
- K. E. Sung, X. Su, E. Berthier, C. Pehlke, A. Friedl, and D. J. Beebe, *PLoS One*, 2013, **8**, e76373.
- S. Kumar, T. S. Shabi, and E. Goormaghtigh, *PLoS One*, 2014, **9**, e111137.
- S. E. Holton, M. J. Walsh, A. Kajdacsy-Balla, and R. Bhargava, *Biophys. J.*, 2011, **101**, 1513–21.
- I. Lühr, A. Friedl, T. Overath, A. Tholey, T. Kunze, F. Hilpert, S. Sebens, N. Arnold, F. Rösel, H.-H. Oberg, N. Maass, C. Mundhenke, W. Jonat, and M. Bauer, *Cancer Lett.*, 2012, **325**, 175–88.
- E. Ioachim, A. Charchanti, E. Briasoulis, V. Karavasilis, H. Tsanou, D. L. Arvanitis, N. J. Agnantis, and N. Pavlidis, *Eur. J. Cancer*, 2002, **38**, 2362–70.
- R. Poincloux, F. Lizárraga, and P. Chavrier, *J. Cell Sci.*, 2009, **122**, 3015–24.
- J. Han, H. Chang, O. Giricz, G. Y. Lee, F. L. Baehner, J. W. Gray, M. J. Bissell, P. A. Kenny, and B. Parvin, *Plos Comput. Biol.*, 2010, **6**.
- P. A. Kenny, G. Y. Lee, C. A. Myers, R. M. Neve, J. R. Semeiks, P. T. Spellman, K. Lorenz, E. H. Lee, M. H. Barcellos-Hoff, O. W. Petersen, J. W. Gray, and M. J. Bissell, *Mol. Oncol.*, 2007, **1**, 84–96.
- K. J. Martin, D. R. Patrick, M. J. Bissell, and M. V Fournier, *PLoS One*, 2008, **3**.
- A. Benard, C. Desmedt, M. Smolina, P. Szternfeld, M. Verdonck, G. Rouas, N. Kheddoumi, F. Rothé, D. Larsimont, C. Sotiriou, and E. Goormaghtigh, *Analyst*, 2014, **139**, 1044–56.
- S. Kumar, C. Desmedt, D. Larsimont, C. Sotiriou, and E. Goormaghtigh, *Analyst*, 2013, **138**, 4058–65.
- S. E. Holton, A. Bergamaschi, B. S. Katzenellenbogen, and R. Bhargava, *PLoS One*, 2014, **9**, e96878.
- M. Smolina and E. Goormaghtigh, *Analyst*, 2015, **140**, 2336–43.
- C. Petibois and G. Deleris, *Trends Biotechnol.*, 2006, **24**, 455–462.
- G. J. Ooi, J. Fox, K. Siu, R. Lewis, K. R. Bambery, D. McNaughton, and B. R. Wood, *Med. Phys.*, 2008, **35**, 2151–61.
- R. M. Neve, K. Chin, J. Fridlyand, J. Yeh, F. L. Baehner, T. Fevr, L. Clark, N. Bayani, J.-P. Coppe, F. Tong, T. Speed, P. T. Spellman, S. DeVries, A. Lapuk, N. J. Wang, W.-L. Kuo, J. L. Stilwell, D. Pinkel, D. G. Albertson, F. M. Waldman, F. McCormick, R. B. Dickson, M. D. Johnson, M. Lippman, S. Ethier, A. Gazdar, and J. W. Gray, *Cancer Cell*, 2006, **10**, 515–27.
- D. L. Holliday and V. Speirs, *Breast Cancer Res.*, 2011, **13**, 215.
- T. Vargo-Gogola and J. M. Rosen, *Nat. Rev. Cancer*, 2007, **7**, 659–672.
- H. K. Kleinman and G. R. Martin, *Semin. Cancer Biol.*, 2005, **15**, 378–86.
- G. Y. Lee, P. A. Kenny, E. H. Lee, and M. J. Bissell, *Nat. Methods*, 2007, **4**, 359–365.
- P. Bassan, A. Kohler, H. Martens, J. Lee, E. Jackson, N. Lockyer, P. Dumas, M. Brown, N. Clarke, and P. Gardner, *J. Biophotonics*, 2010, **3**, 609–20.
- P. Bassan, A. Sachdeva, A. Kohler, C. Hughes, A. Henderson, J. Boyle, J. H. Shanks, M. Brown, N. W. Clarke, and P. Gardner, *Analyst*, 2012, **137**, 1370–7.
- B. Bird, M. Miljković, and M. Diem, *J. Biophotonics*, 2010, **3**, 597–608.
- K. R. Bambery, B. R. Wood, and D. McNaughton, *Analyst*, 2012, **137**, 126–32.
- A. Dazzi, A. Deniset-Besseau, and P. Lasch, *Analyst*, 2013, **138**, 4191–201.
- A. Gaigneaux, J. M. Ruyschaert, and E. Goormaghtigh, *Appl. Spectrosc.*, 2006, **60**, 1022–1028.
- M. J. Bissell, D. C. Radisky, A. Rizki, V. M. Weaver, and O. W. Petersen, *Differentiation*, 2002, **70**, 537–546.
- Z. I. Khamis, Z. J. Sahab, and Q.-X. A. Sang, *Int. J. Breast Cancer*, 2012, **2012**, 574025.
- M. H. Barcellos-Hoff and D. Medina, *Breast Cancer Res.*, 2005, **7**, 33–6.
- N. A. Bhowmick, E. G. Neilson, and H. L. Moses, *Nature*, 2004, **432**, 332–7.
- W. H. Fridman, J. Galon, F. Pagès, E. Tartour, C. Sautès-Fridman, and G. Kroemer, *Cancer Res.*, 2011, **71**, 5601–5.
- D. Liao, Y. Luo, D. Markowitz, R. Xiang, and R. A. Reisfeld, *PLoS One*, 2009, **4**, e7965.
- A. D. Meade, C. Clarke, F. Draux, G. D. Sockalingum, M. Manfait, F. M. Lyng, and H. J. Byrne, *Anal. Bioanal. Chem.*, 2010, **396**, 1781–91.
- C. J. Huijsmans, J. Damen, J. C. van der Linden, P. H. Savelkoul, and M. H. Hermans, *BMC Res. Notes*, 2010, **3**, 239.

ARTICLE

Journal Name

- 1
2
3
4
5
6
7
8
9
10
11
12
13
14
15
16
17
18
19
20
21
22
23
24
25
26
27
28
29
30
31
32
33
34
35
36
37
38
39
40
41
42
43
44
45
46
47
48
49
50
51
52
53
54
55
56
57
58
59
60
36. M. Braun, R. Menon, P. Nikolov, R. Kirsten, K. Petersen, D. Schilling, C. Schott, S. Gündisch, F. Fend, K.-F. Becker, and S. Perner, *BMC Cancer*, 2011, **11**, 511.
37. D. L. Evers, C. B. Fowler, B. R. Cunningham, J. T. Mason, and T. J. O'Leary, *J. Mol. Diagn.*, 2011, **13**, 282–8.
38. D. Otali, C. R. Stockard, D. K. Oelschlager, W. Wan, U. Manne, S. A. Watts, and W. E. Grizzle, 2010, **84**, 223–247.
39. E. Gazi, J. Dwyer, N. P. Lockyer, J. Miyan, P. Gardner, C. Hart, M. Brown, and N. W. Clarke, *Biopolymers*, 2005, **77**, 18–30.
40. N. L. Pleshko, a L. Boskey, and R. Mendelsohn, *Calcif. Tissue Int.*, 1992, **51**, 72–7.
41. M. M. Mariani, P. Lampen, J. Popp, B. R. Wood, and V. Deckert, *Analyst*, 2009, **134**, 1154–1161.
42. A. I. Mazur, E. J. Marcsisin, B. Bird, M. Miljkoviš, and M. Diem, *Anal. Chem.*, 2012, **84**, 1259–1266.
43. A. I. Mazur, E. J. Marcsisin, B. Bird, M. Miljković, and M. Diem, *Anal. Chem.*, 2012, **84**, 8265–71.
44. G. Hastings, R. Wang, P. Krug, D. Katz, and J. Hilliard, *Biopolymers*, 2008, **89**, 921–30.
45. A. C. Bot, A. Huizinga, F. F. de Mul, G. F. Vrensen, and J. Greve, *Exp. Eye Res.*, 1989, **49**, 161–9.
46. E. O'Faolain, M. Hunter, J. Byrne, P. Kellehan, M. McNamara, and F. Lying, *Dublin Inst. Technol.*, 2005, **38**, 121–127.
47. Z. Huang, A. McWilliams, S. Lam, J. English, D. I. McLean, H. Lui, and H. Zeng, *Int. J. Oncol.*, 2003, **23**, 649–55.
48. D. C. Fernandez, R. Bhargava, S. M. Hewitt, and I. W. Levin, *Nat. Biotechnol.*, 2005, **23**, 469–474.
49. R. Bhargava, *Anal. Bioanal. Chem.*, 2007, **389**, 1155–69.
50. M. Verdonck, N. Wald, J. Janssis, P. Yan, C. Meyer, A. Legat, D. E. Speiser, C. Desmedt, D. Larsimont, C. Sotiriou, and E. Goormaghtigh, *Analyst*, 2013, **137**, 3255–64.
51. M. G. Shim and B. C. Wilson, *Photochem. Photobiol.*, 1996, **63**, 662–71.
52. E. Goormaghtigh, V. Cabiaux, and J. M. Ruysschaert, *Subcell. Biochem.*, 1994, **23**, 405–450.
53. E. Goormaghtigh, R. Gasper, A. Benard, A. Goldsztein, V. Raussens, and A. Bénard, *Biochim Biophys. Acta-Proteins Proteomics*, 2009, **1794**, 1332–1343.
54. E. Goormaghtigh, J. M. Ruysschaert, and V. Raussens, *Biophys. J.*, 2006, **90**, 2946–2957.
55. C.-L. Chiu, M. A. Digman, and E. Gratton, *J. Biophys.*, 2013, **2013**, 532030.